RSC Advances

PAPER

View Article Online
View Journal | View Issue

Cite this: *RSC Adv.*, 2026, **16**, 8945

Colchicine–cinnamic acid hybrids with potent anticancer activities: synthesis, *in vitro*, and *in vivo* biological evaluations

Xiaoqin Li,[abc] Nan Li,[d] Mei Zhang,[abc] Shengqi Deng,[d] Lin Zheng,[d] Yang Chen*[d] and Shumei Wang *[aefg]

Cancer represents a critical global health burden, with the clinical application of many chemotherapeutic agents constrained by limited efficacy and significant toxicity. Colchicine, a tubulin-targeting agent, exhibits potent anticancer activity but has a narrow therapeutic window. Conversely, natural cinnamic acid and its derivatives are safe but lack strong antitumor potency and specific targets. To resolve this "potency-toxicity" paradox, a series of colchicine–cinnamic acid hybrids (**B1–B12**) were designed and synthesized *via* molecular hybridization, aiming to integrate the strong tubulin-binding activity of colchicine with the biocompatibility of cinnamic acids. Among these derivatives, **B3**, **B6**, **B7**, and **B8** showed pronounced cytotoxic activity against B16, 4T1, A549, and HepG2 cancer cell lines. Notably, compound **B7** emerged as the most effective, with an IC_{50} range of 2.5–8.1 nM and excellent selectivity indexes (SI) of 112 against A549 and 55 against HepG2. Further mechanistic studies revealed that **B7** effectively disrupted microtubule dynamics in 4T1 cells, induced G2/M-phase cell-cycle arrest, and triggered apoptosis, thereby inhibiting cell proliferation and migration. Molecular docking studies suggested that **B7** occupies the colchicine-binding site at the α/β-tubulin interface. In a 4T1 murine breast tumor model, **B7** showed significant *in vivo* antitumor efficacy, achieving a 68.4% tumor growth inhibition (TGI) at 0.6 mg $kg^{-1}day^{-1}$, with a favorable safety profile. These results suggest that colchicine–cinnamic acid hybrids, particularly **B7**, represent a promising class of lead compounds for developing novel anticancer agents.

Received 1st December 2025
Accepted 6th February 2026

DOI: 10.1039/d5ra09278g

rsc.li/rsc-advances

1 Introduction

Cancer is a globally devastating disease burdening public health. Based on updated estimates from the International Agency for Research on Cancer (IARC), there were approximately 20 million new cancer cases and 9.7 million cancer-related deaths worldwide, reflecting the persistently heavy burden of this disease.[1] The incidence and mortality of cancer rise annually due to aging, pollution, and unhealthy lifestyles. Although there are advances in treatments like surgery, chemotherapy, and immunotherapy, the prognosis for patients with advanced or metastatic cancer remains poor. In particular, chemotherapy, as a primary cancer treatment, still suffers from systemic toxicity, drug resistance, and a lack of tumor selectivity. Therefore, novel anticancer agents with high potency, good selectivity, and low toxicity are urgently needed.

Natural products and their derivatives are privileged sources of anticancer lead compounds due to their structural diversity and unique bioactivities. Among them, colchicine (**1**, Fig. 1), a tricyclic alkaloid derived from Colchicum autumnale, is a well-characterized tubulin-binding agent. It acts by inhibiting microtubule polymerization, disrupting cytoskeletal dynamics, and inducing G2/M cell cycle arrest and apoptosis in proliferating cells. Colchicine has demonstrated promising anticancer potential against breast cancer, lung cancer, and leukemia models. However, its clinical utility is severely limited by significant toxicity (including gastrointestinal, bone marrow, and hepatic side effects) and a narrow therapeutic window. Meanwhile, cinnamic acid (**2**, Fig. 1), a natural product with a long history of safe human exposure, possesses a unique α,β-

[a]*School of Pharmacy, Chengdu University of Traditional Chinese Medicine, Chengdu, China. E-mail: gdpuwsm@126.com*

[b]*Key Laboratory of Standardization of Chinese Medicine (Chengdu University of Traditional Chinese Medicine), Ministry of Education, Chengdu, China*

[c]*Chinese Medicine Germplasm Resources Innovation and Effective Uses Key Laboratory of Sichuan Province, Chengdu, China*

[d]*Antibiotics Research and Re-evaluation Key Laboratory of Sichuan Province, School of Pharmacy, Chengdu University, Chengdu, China. E-mail: chenyang1@cdu.edu.cn*

[e]*School of Chinese Materia Medica, Guangdong Pharmaceutical University, Guangzhou, China*

[f]*Key Laboratory of Digital Quality Evaluation of Chinese Materia Medica of State Administration of TCM, School of Chinese Materia Medica, Guangdong Pharmaceutical University, Guangzhou, China*

[g]*Engineering & Technology Research Center for Chinese Materia Medica Quality of the Universities of Guangdong Province, School of Chinese Materia Medica, Guangdong Pharmaceutical University, Guangzhou, China*

unsaturated carbonyl structure that confers a broad range of pharmacological activities.[2,3] Notably, numerous cinnamic acid derivatives bearing various substituents have been reported to exhibit potent antiproliferative effects against a wide range of tumor cell lines through diverse mechanisms,[4–6] making them not only benign linkers but also attractive pharmacophores for rational anticancer drug design *via* hybridization.

To address the "potency-toxicity" dilemma inherent to colchicine-based therapy, we adopted a molecular hybridization strategy.[7,8] This well-established drug design approach integrates pharmacophoric elements from distinct bioactive molecules into a single hybrid structure, aiming to combine their beneficial properties while mitigating individual limitations. In this context, we hypothesized that conjugating the potent tubulin-targeting scaffold of colchicine with the structurally varied, low-toxicity, yet intrinsically bioactive frameworks of cinnamic acid derivatives could yield novel chemical entities with optimized anticancer profiles.

The design of the target hybrids was guided by a careful analysis of the structure–activity relationship (SAR) of colchicine. Previous SAR studies have demonstrated that: (1) the methoxy groups on ring A are critical for maintaining high affinity to the colchicine-binding site on tubulin;[9] (2) the C-4 position is highly sensitive to substitution,[10–12] with bulky groups often leading to undesirable loss of both potency and toxicity;[13,14] (3) ring C is crucial for tubulin interaction, and steric bulk at the C-10 position generally reduces antitumor activity; (4) the B-ring, particularly the C-7 position, is tolerant to modification without disrupting the core tubulin-binding function.[15] Importantly, the amine group at C-7 has been widely used for conjugation, allowing modulation of pharmacokinetic and pharmacodynamic properties.[16]

Based on this rationale, we focused on the C-7 position of colchicine as the optimal site for structural diversification. We designed and synthesized a novel series of colchicine–cinnamic acid hybrids (**B1–B12**) by covalently linking cinnamic acid and selected analogues to the C-7 amine *via* a condensation reaction. This series represents a systematic exploration of structure–activity relationships, in which the colchicine core is maintained, and the cinnamic acid moiety is varied to investigate its contribution. This strategic hybridization aims to preserve colchicine's potent microtubule-disrupting activity while introducing a favorable safety profile and the potential for additional, synergistic bioactivity from cinnamic acid pharmacophores. We hypothesize that such hybrids may exhibit enhanced tumor selectivity, improved therapeutic windows, and retained or even augmented antiproliferative efficacy through possible multi-modal action.

Thus, the present study systematically evaluates the antitumor potential of these newly synthesized hybrids to identify promising lead compounds that effectively balance high potency with reduced toxicity—a critical step toward the development of novel, and more clinically viable tubulin-targeting agents.

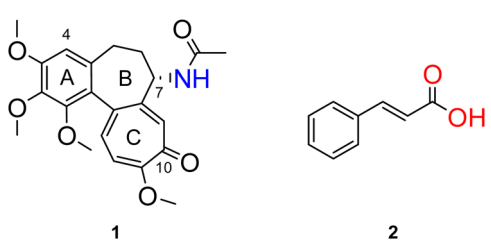

Fig. 1 Natural product colchicine (**1**) and cinnamic acid (**2**).

2 Results and discussion

2.1. Chemistry

The synthetic route for preparing the novel C-7-modified derivatives is illustrated in Scheme 1. The synthesis began with the preparation of *N*-deacetylcolchicine (**3**) *via* a three-step sequence: *N*-Boc protection, deacetylation, and subsequent Boc deprotection. This route was specifically adopted to ensure clean, efficient preparation of the key intermediate. The C7 acetamido group of colchicine can be hydrolyzed under forcing acidic conditions, which induces C-ring isomerization and requires tedious purification.[17] To avoid such isomerization, we adopted a three-step method based on a published procedure[18] to synthesize *N*-deacetylcolchicine. Therefore, temporary Boc protection was employed to shield the secondary amine group (–NH–) during the deacetylation step, preventing undesired side reactions (*e.g.*, intramolecular aminolysis) and ensuring a high yield of the intermediate. Following deacetylation, mild acidic removal of the Boc group cleanly regenerated the free amine, furnishing *N*-deacetylcolchicine (**3**) in good overall yield and purity, ready for subsequent condensation.

With intermediate **3** in hand, the target colchicine–cinnamic acid hybrids **B1–B12**(Chart 1)were synthesized *via* an amide coupling strategy. The condensation reactions between *N*-deacetylcolchicine (**3**) and the respective cinnamic acid analogs

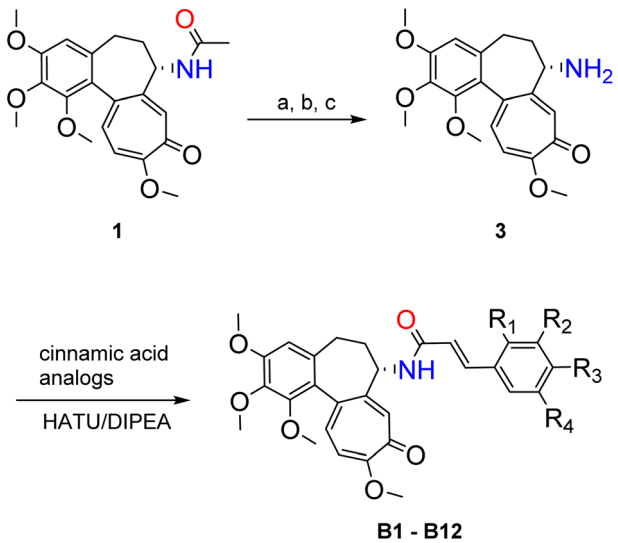

Scheme 1 Synthesis of colchicine-cinnamic acid hybrids. Reagents and conditions: (a) Boc_2O, DMAP, Et_3N, CH_3CN, reflux, 20 h; (b) MeONa, MeOH, 0 °C, 1 h; (c) TFA, DCM, rt, 3 h. See Chart 1 for structures and isolated yields.

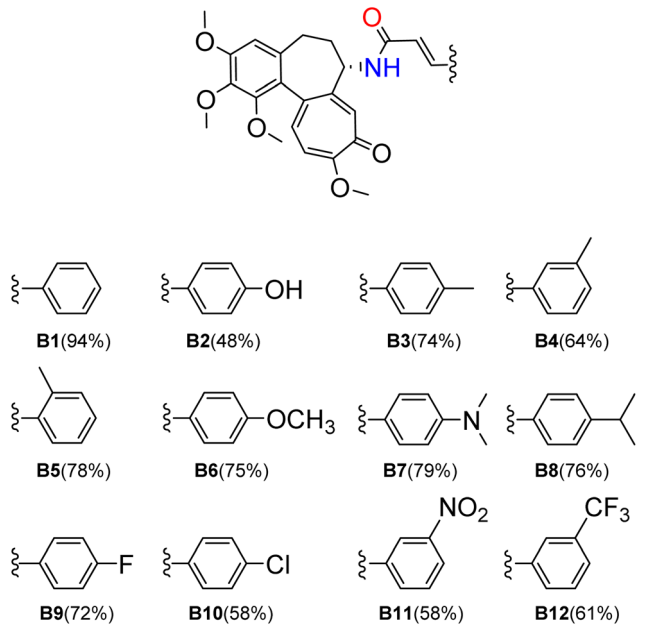

Chart 1 New colchicine-cinnamic acid hybrids were synthesized according to Scheme 1. Yields of purified products are given in brackets.

were performed using HATU as the coupling agent in anhydrous dichloromethane, under an inert atmosphere at room temperature. These conditions were optimized to achieve efficient amide bond formation while minimizing epimerization or decomposition of the sensitive colchicine scaffold. After standard aqueous workup and purification by silica gel column chromatography, compounds **B1–B12** were obtained in moderate to good yields (48–94%). All final compounds were fully characterized by ^{1}H NMR, ^{13}C NMR, and HRMS, and the spectral data were consistent with the assigned structures.

Table 1 IC_{50} values of colchicine and its novel derivatives against B16 cells and 4T1 cells[a]

	IC_{50} values (nM)	
Compounds	B16	4T1
1	35.3 ± 5.0	46.0 ± 4.1
2	8288.3 ± 1244.0	>100 000
3	67.3 ± 3.4	66.6 ± 4.4
B1	97.6 ± 11.0	211.0 ± 15.6
B2	262.5 ± 30.4	443.5 ± 18.5
B3	9.3 ± 0.6	29.3 ± 1.1
B4	204.6 ± 21.4	323.2 ± 32.3
B5	327.9 ± 27.5	499.1 ± 27.2
B6	3.8 ± 0.7	18.1 ± 1.8
B7	2.5 ± 0.3	2.6 ± 0.3
B8	7.6 ± 0.5	26.4 ± 1.7
B9	115.6 ± 17.1	247.7 ± 16.8
B10	165.8 ± 8.4	303.6 ± 21.5
B11	92.6 ± 5.0	178.9 ± 23.0
B12	145.0 ± 19.3	268.1 ± 11.1

[a] Values represent cytotoxic activity (the half-maximal inhibitory concentration, IC_{50}) after 72 h test compound incubation. Data shown are mean values ± SD from at least three independent experiments.

The design of the hybrid series followed a systematic structure–activity relationship (SAR) exploration. Initially, derivatives **B1–B3** were prepared from naturally abundant cinnamic acid analogs to evaluate the influence of simple phenyl ring substitution. Subsequently, compounds **B4** and **B5** were synthesized to probe the effect of substituent position (*ortho*, *meta*, *para*) on biological activity. Further structural optimization was pursued by modulating electronic properties and polarity, yielding analogs **B6–B12** that bear various functional groups, including halogens, methoxy, and nitro substituents. This graded synthetic approach enabled a coherent assessment of how structural changes to the cinnamic acid moiety affect the anticancer potency and selectivity of the resulting hybrids.

2.2. *In Vitro* research

2.2.1 Cytotoxicity against B16 cells and 4T1 cells. Cytotoxicity (half-maximal inhibitory concentration, IC_{50}) of all derivatives against B16 and 4T1 cells was used as a reference for structural modification and was determined by the MTT assay. The IC_{50} values presented in Table 1 indicate a decrease in cytotoxicity for *N*-deacetylcolchicine (**3**), while cinnamic acid (**2**) exhibited a relatively mild inhibitory effect. However, when these two compounds are condensed, it results in notable changes in the toxicity of the hybrid. Including cinnamic acid and its analogs significantly altered the cytotoxicity of these colchicine–cinnamic acid amides, yet they still retained some antiproliferative properties. Among the four initially synthesized derivatives (**B1–B3**), **B3** exhibited the highest cytotoxic activity and could inhibit cell growth even at low nanomolar concentrations (IC_{50} [B16] = 9.3 nM, IC_{50} [4T1] = 29.3 nM). At the same time, the differences in activity between **B1–B3** suggested that substituents on the benzene ring had a significant impact on activity.

Among the methyl-substituted analogs **B3–B5**, the *para*-methyl derivative **B4** exhibited the most potent and significantly enhanced activity. This suggests that *para*-substitution with an electron-donating group, such as a methyl group, is favorable for improving the antiproliferative activity relative to the parent cinnamic acid derivative **B1**. Then, the cell viability assay of derivatives **B6–B10** substituted at the *para*-position with various electronic effects was performed to verify this conjecture. In the case of *para*-substituted derivatives, the electron-withdrawing groups such as *p*-F and *p*-Cl reduced activity, whereas the electron-donating groups *p*-$N(CH_3)_2$, *p*-$C(CH_3)_2$, and *p*-OCH_3 significantly increased cytotoxicity. In particular, the *p*-$N(CH_3)_2$ substituted compound **B7** demonstrated the most potent cytotoxic activity (IC_{50} [B16] = 2.5 nM, IC_{50} [4T1] = 2.6 nM), which is in line with the strong electron-donating character of the dimethylamine group. Therefore, it may be concluded that introducing an electron-donating group in the *para*-position of the designed derivatives is more beneficial for increased antitumor activity, and the improved electron-donating capacity correlates with higher potency.

To further investigate the impact of benzene ring substituents on activity, electron-withdrawing groups were introduced at the *meta*-position of the benzene ring. It was observed that

Table 2 IC_{50} values of colchicine and active derivatives against A549, HepG2, and L929 cells (mean ± SD, $n = 3$)

Compounds	IC_{50} values (nM)			Selectivity index (SI)	
	A549	HepG2	L929	A549	HepG2
1	39.6 ± 1.9	46.6 ± 5.8	425.7 ± 36.3	11	9
B3	11.2 ± 1.3	21.5 ± 0.8	730.1 ± 60.2	65	34
B6	9.4 ± 1.5	16.3 ± 1.9	441.8 ± 43.8	47	27
B7	4.0 ± 0.6	8.1 ± 0.8	446.1 ± 14.4	112	55
B8	7.3 ± 1.6	17.0 ± 1.7	376.3 ± 26.6	52	22

the antitumor activity of the *meta*-substituted compounds (**B4**, **B11**, and **B12**) increased with the stronger electron-withdrawing ability of the substituents (*m*-CH_3, *m*-CF_3, and *m*-NO_2). However, it is important to note that the activity of all three compounds was notably lower than that of the unsubstituted compound. This finding underscores the critical role of the electronic properties of benzene ring substituents, as well as the close correlation between the substituent position and the inhibitory activity against tumor cells.

2.2.2 Selectivity index (SI) values of active derivatives. The above experimental results showed that derivatives **B3**, **B6**, **B7**, and **B8** exhibited greater cytotoxicity than colchicine against animal cancer cells. This means these derivatives may have higher anti-cancer potential. Further investigation was conducted to evaluate the effects of these active derivatives on the growth of human tumor cell lines (HepG2 and A549) and normal cell lines (L929). This research aims to confirm their effects on human cancer cells and assess their selectivity by comparing IC_{50} values with those for normal cells. The mean IC_{50} ± SD of the tested compounds is collected in Table 2.

Based on the primary analysis of the IC_{50} values in Table 2, the inhibitory effects of the tested derivatives on human cancer cells are consistent with those observed in animal cancer cells. Additionally, compound **B7** exhibited significant cytotoxicity against A549 cells ($IC_{50} = 4.0$ nM) and HepG2 cells ($IC_{50} = 8.1$ nM), which were 10-fold and 6-fold higher than those of colchicine, respectively. At this stage, the cytotoxicity of the active derivatives has been demonstrated, indicating that these compounds exhibit more potent antitumor activity than colchicine. Further analysis was conducted to determine their therapeutic potential by comparing the IC_{50} values of cancer cells and normal cells to calculate the selectivity index (SI). This is illustrated in Fig. 2.

The selectivity index is an important indicator used to measure the difference in drug effects on target and normal cells. This difference can reflect the specific antitumor activity of drugs against tumor cells compared with normal cells. By comparing the IC_{50} values of these two cell types, we can preliminarily evaluate drug selectivity for tumor treatment. As shown in Fig. 2, derivatives **B3**, **B6**, **B7**, and **B8** exhibited higher SI values for A549 and HepG2 cell lines in comparison to colchicine. Moreover, compound **B7** stands out with its exceptional SI value and remarkable ability to inhibit the proliferation of A549 and HepG2 cell lines. The impressive performance of this compound makes it an excellent candidate for further research.

2.2.3 Comparison of the cytotoxicity of B7 and its starting material. Compound **B7** is a potent compound that has been synthesized by combining *N*-deacetylcolchicine (**3**) and 4-(dimethylamino) cinnamic acid (**4**) through a condensation reaction. When combined, it is essential to consider the potential additive or synergistic effects of these two molecules, as the resulting compound could have even greater efficacy and potency than the individual molecules. To this end, the cytotoxicity of the intermediate **3**, the acid **4**, and the hybrid **B7** was

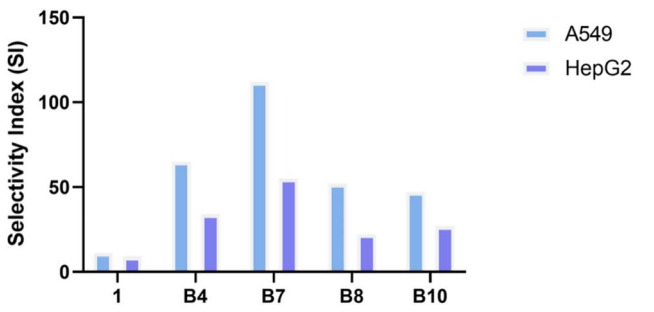

Fig. 2 Selectivity index (SI) values of tested compounds. The SI value was calculated for each compound using the formula: SI=IC_{50} [L929]/IC_{50} [A549], or SI=IC_{50} [L929]/IC_{50} [HepG2].

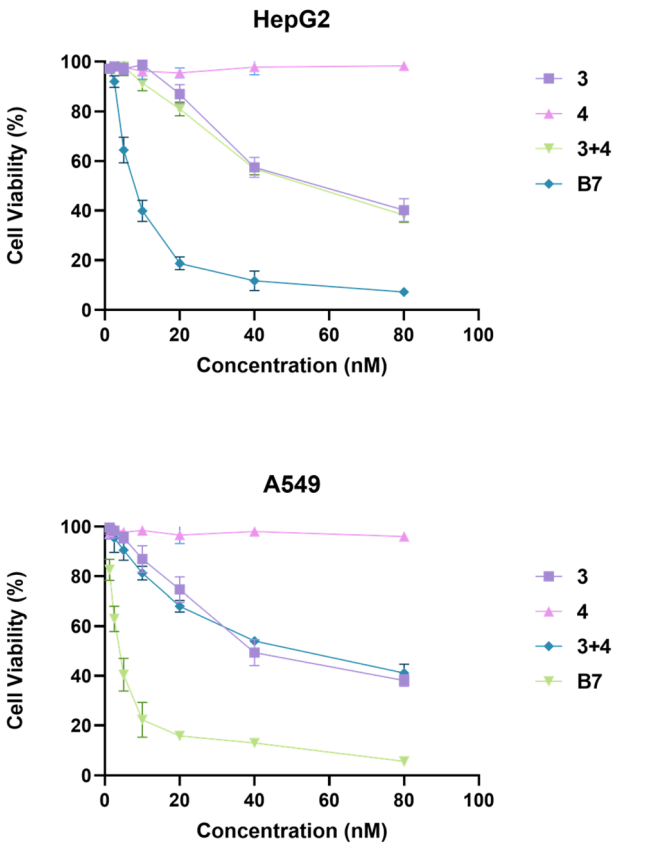

Fig. 3 The cytotoxicity of compounds **3** and **4**, and their combination (**3+4**, a mixture of **3** and **4** with a mole ratio 1 : 1) on human tumor cell lines (HepG2 and A549 cells) and comparison with compound **B7**.

assessed individually against the human tumor cell lines HepG2 and A549. The results, presented in Fig. 3, clearly demonstrate that **B7** exhibits significantly greater potency than either **3** or **4** alone, supporting the synergistic benefit of the molecular hybridization strategy.

Based on the observations, **B7** has a much greater inhibitory effect on cell growth than compounds **3**, **4**, or their combination (**3+4**) at low nanomolar concentrations (≤10 nM). The findings have proven that the high activity of **B7** is not solely due to additive or synergistic effects. Overall, the study emphasizes the potential of compound **B7** in combating cancer.

2.2.4 The effect of B7 on the proliferation and migration of 4T1 cells. The further study aimed to investigate the antitumor potential of compound **B7** by examining its effect on the proliferation and migration of 4T1 cells. The colony formation assay was performed on 4T1 cells treated with **B7** at 0, 2.5, or 10 nM and with colchicine at 10 nM for 10 days. The assay aimed to evaluate the impact of these treatments on cell proliferation. As shown in Fig. 4A and B, colony size and 4T1 cell number were visibly reduced in cells treated with 2.5 nM **B7** compared to the control group (0 nM). The group treated with 10 nM **B7** showed very few colonies. The effect of **B7** on degenerated proliferation was particularly noticeable at 10 nM compared to colchicine.

Moreover, to examine the impact of **B7** on 4T1 cell migration, an *in vitro* wound-healing assay was conducted after treatment with 10 nM **B7** or colchicine (Fig. 4C and D). The findings revealed that the migration area of 4T1 cells treated with **B7** or colchicine for 12 hours decreased by 43.7% and 19.7%, respectively, compared with the control group (0 nM). After 24 hours of administration, the migration area in the **B7** group decreased by 30.3%, whereas it decreased by only 12.3% in the colchicine group. This suggests that **B7** exhibits a more pronounced inhibitory effect on 4T1 cell migration than colchicine. The results of the colony formation and wound-healing assays demonstrated that compound **B7** has significant antitumor potential, as it inhibits both cancer cell proliferation and migration.

2.2.5 Cell cycle analysis. Disruptions in microtubule dynamics during cell division can lead to mitotic arrest. To further validate the mechanism of **B7**, flow cytometry was used to examine its effects on the cell cycle of 4T1 cells. The cells were treated with 5 nM, 10 nM, and 15 nM of **B7** for 24 h, and the distribution of 4T1 cells across different stages of the cell cycle was analysed post-treatment. As shown in Fig. 5, the proportion of cells in the G2/M phase increased with increasing compound **B7** concentration. Notably, following treatment with 15 nM **B7**, 82.44% of 4T1 cells were in the G2/M phase, a 68.73% increase over the control group (0 nM **B7**). These findings suggest that compound **B7** effectively induces G2/M phase arrest in 4T1 cells.

2.2.6 Effect of B7 on cell apoptosis. Arresting the cell cycle at the G2/M phase inhibits cell proliferation and promotes apoptosis. To investigate the effect of **B7** on cell apoptosis, Annexin V/PI double staining was performed on 4T1 cells, and

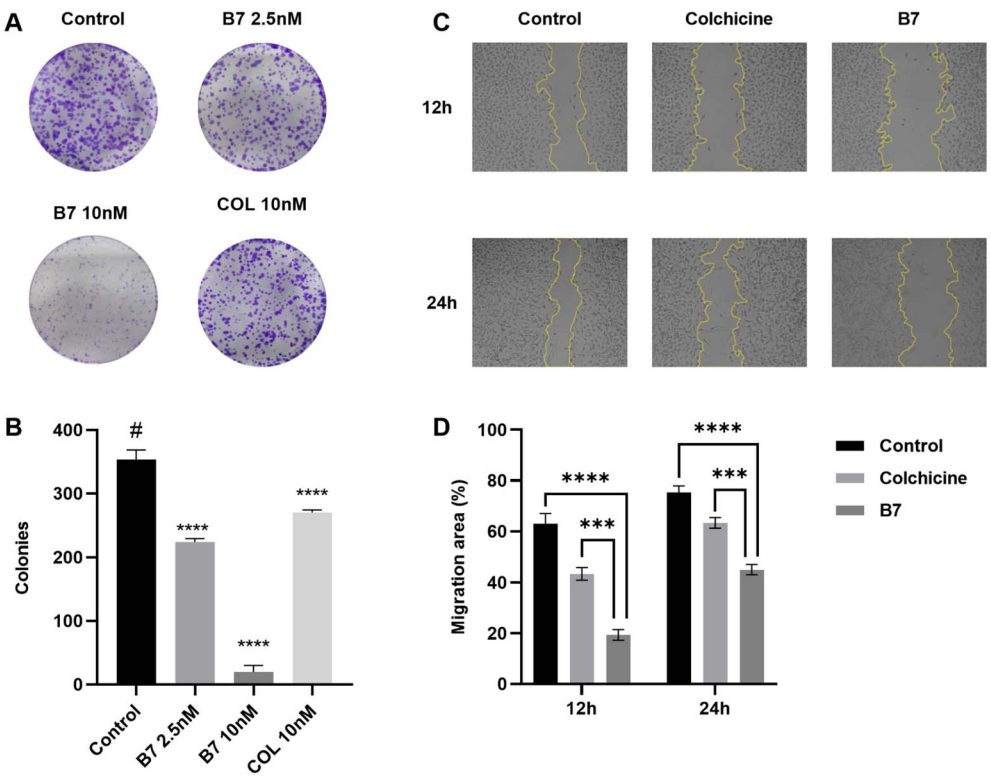

Fig. 4 The effect of compound **B7** on the proliferation and migration ability of 4T1 cells. (A) Proliferation in 4T1 cells incubated with **B7** (0, 2.5, and 10 nM) or colchicine (10 nM) was assessed by the colony-forming assay. (B) Statistical chart of **B7** inhibiting the clone formation of B16 cells. (C) The migration ability of 4T1 cells incubated with **B7** or colchicine was evaluated by a wound healing assay. (D) Statistical chart of the migration area in the wound healing assay. ***P < 0.001, ****P < 0.0001.

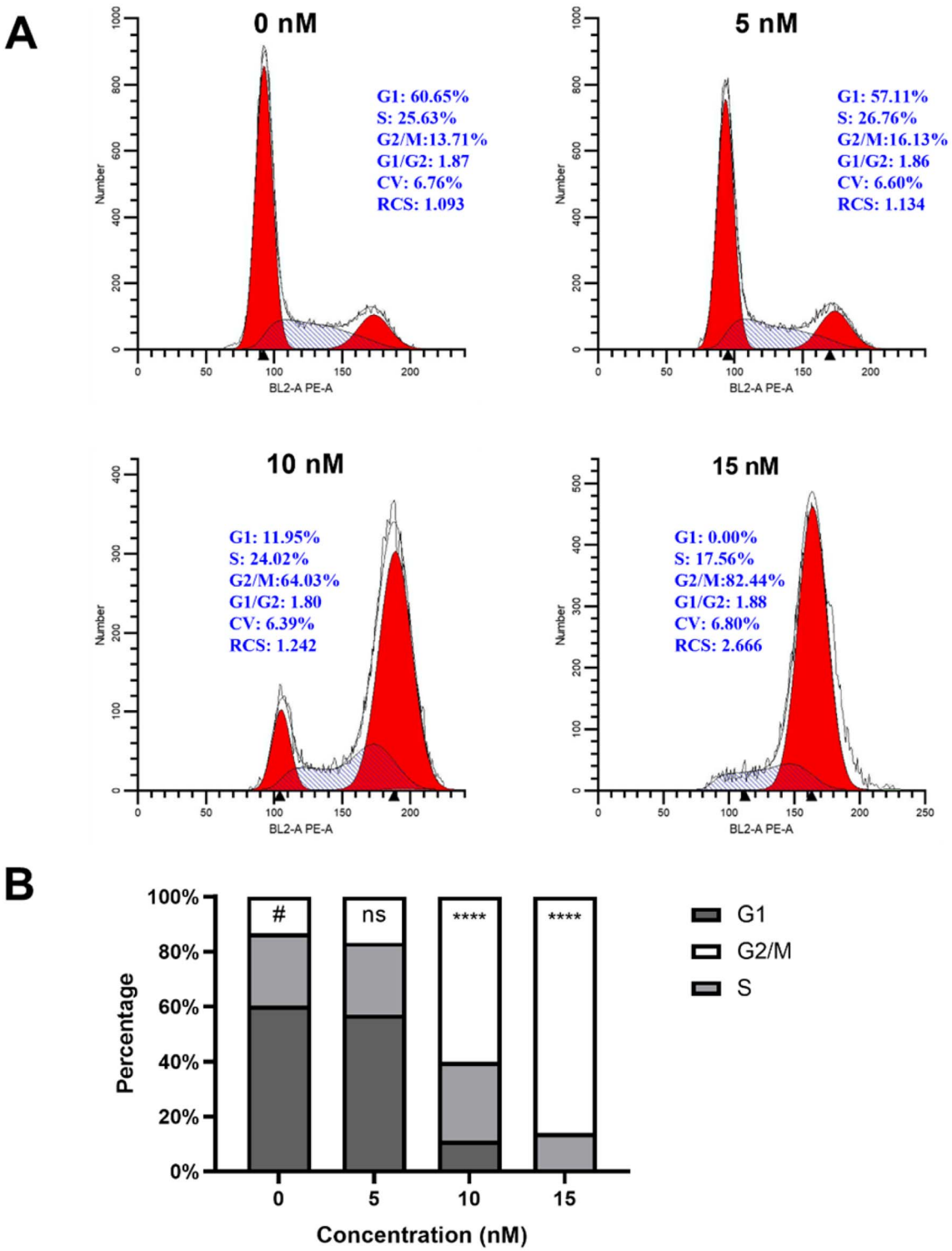

Fig. 5 Effects of compound **B7** on the cell cycle of 4T1 cells. (A) Distribution figures of the cell cycle were representative of three independent experiments. (B) Statistical chart of the proportion of cells in G1, G2/M, and S phases ($n = 3$). Two-way ANOVA followed by Tukey's test was used for (B). ****$P < 0.0001$; ns, not significant.

apoptotic cells were detected by flow cytometry. The results demonstrated a substantial increase in the percentage of apoptotic cells following 48 hours of incubation with **B7** at concentrations of 10 nM and 15 nM (Fig. 6). Statistical analysis indicated significant differences in apoptotic rates between the control group (0 nM **B7**, 2.57 ± 1.04%) and both the 10 nM **B7** group (79.11 ± 4.07%, $P < 0.0001$) and the 15 nM **B7** group (78.10 ± 2.39%, $P < 0.0001$). Thus, **B7** was shown to induce apoptosis in 4T1 cells.

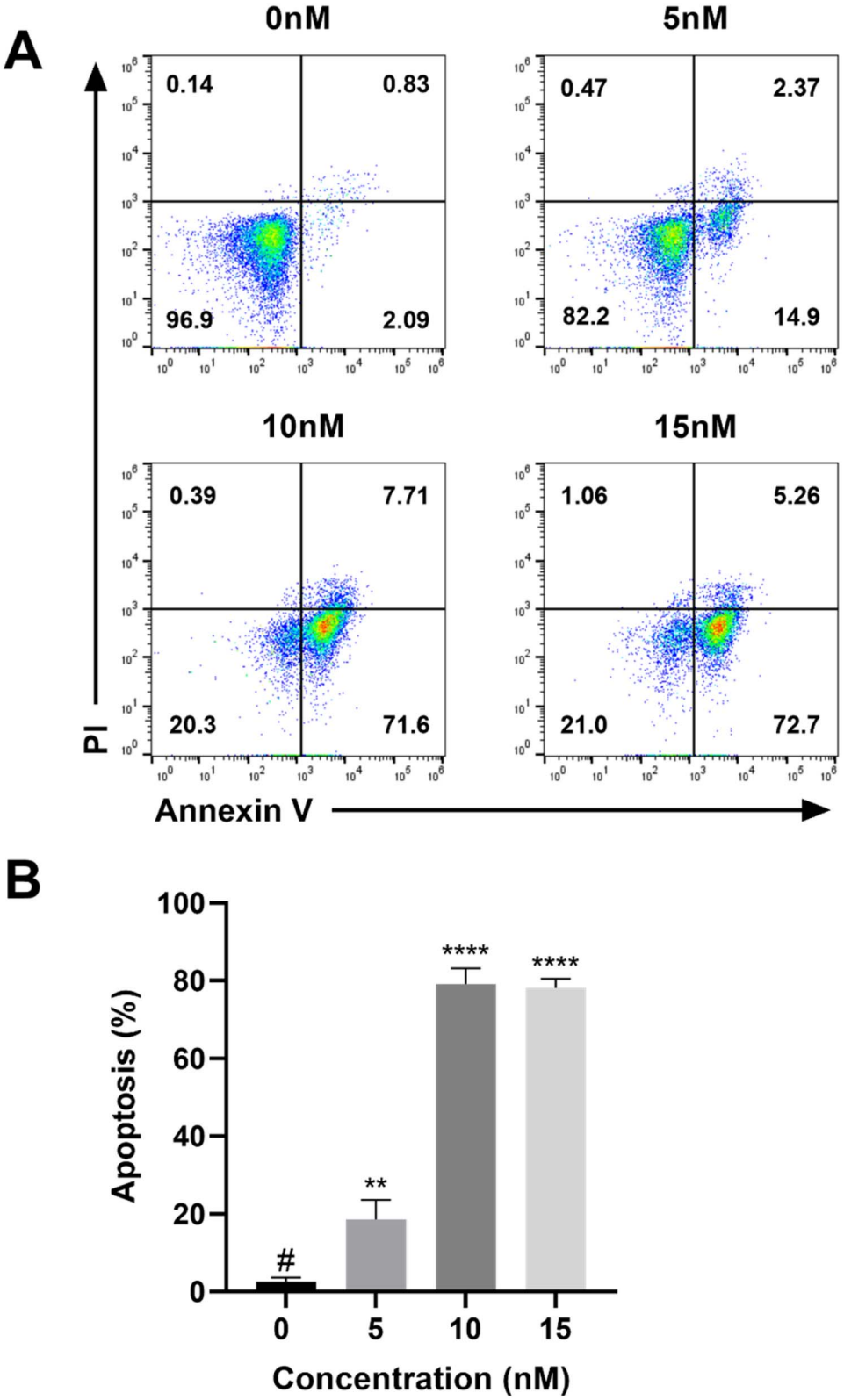

Fig. 6 Effects of compound **B7** on the cell apoptosis of 4T1 cells. (A) The cell apoptosis ratio of treated cells was detected by flow cytometry and calculated by FlowJo. The apoptosis results shown were close to the median of three independent experiments. (B) A graphical illustration of the percentage of total apoptosis, a sum of early-stage (Annexin V+/PI-) and late-stage (Annexin V+/PI+) apoptosis. $^{**}P < 0.01$, $^{****}P < 0.0001$ *vs.* the control group (#).

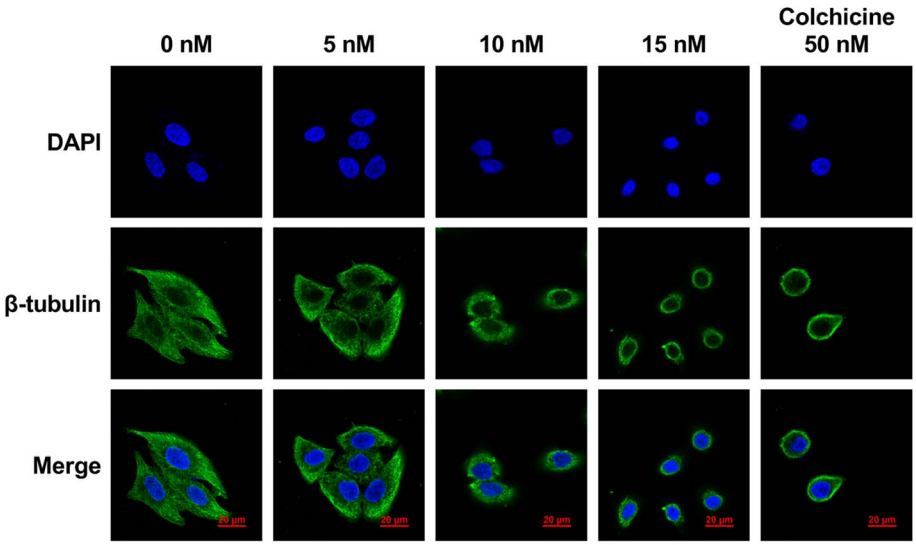

Fig. 7 Effects of **B7** (0, 5, 10, and 15 nM) and colchicine (50 nM) on the cellular microtubule networks assessed by immunofluorescence staining. These images served as a representative of three separate experiments. Microtubules were identified using an anti-β-tubulin antibody in conjunction with a FITC-conjugated secondary antibody (green). The cell nuclei were also visualized using the nucleic acid stain DAPI (blue). Scale bar: 20 μm.

2.3. Mechanism research

2.3.1 Analysis of immunofluorescence staining. To investigate the alignment of the structurally modified compound **B7** with the colchicine mechanism, immunofluorescence staining was employed to evaluate its effects on microtubule dynamics in 4T1 cells. Various concentrations of **B7** (0, 5, 10, and 15 nM) were administered, and the samples were subsequently stained with β-tubulin and DAPI to assess the morphological changes in the 4T1 cell nucleus (blue fluorescence) and the microtubule network (green fluorescence). Colchicine (50 nM) was applied as a positive control for comparative analysis. As illustrated in

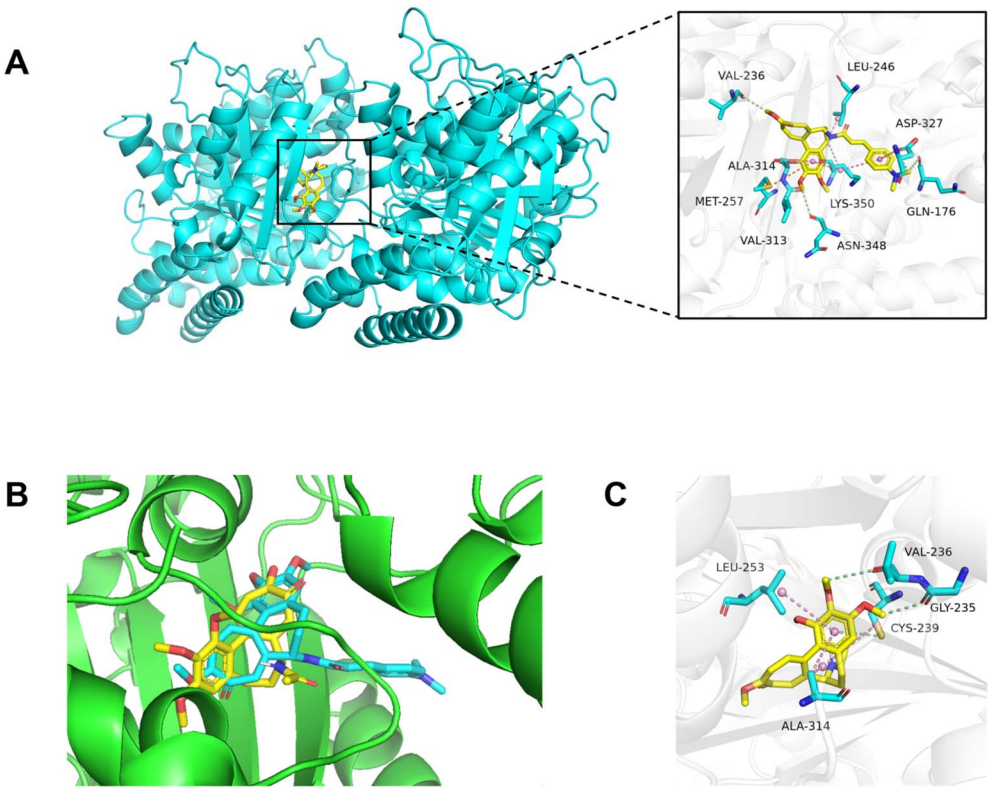

Fig. 8 The binding mode of **B7** with tubulin (PDB ID: 5YLJ). (A) The binding site between **B7** and tubulin. (B) The binding mode of colchicine with tubulin. (C) The overlap between **B7** and colchicine at the colchicine binding domain.

Table 3 Tumor volume, weight, and TGI of each group in mice tumor model (mean ± SD, $n = 6$)

Group	Tumor volume (mm^3)		Tumor weight (g)	TGI (%)
	Pre-treatment	Post-treatment		
Control	93.6 ± 32.0	704.8 ± 150.5	0.51 ± 0.12	—
B7-L	94.84 ± 15.3	456.0 ± 78.0[a]	0.35 ± 0.04	36.2
COL-L	90.2 ± 30.9	538.9 ± 83.2[b]	0.43 ± 0.06	20.6
B7–H	95.6 ± 33.3	227.4 ± 118.1[c,d]	0.20 ± 0.11	68.4
COL-H	89.0 ± 42.0	443.5 ± 136.5[a]	0.38 ± 0.08	33.8
5-FU	91.1 ± 36.8	242.2 ± 142.2[c]	0.26 ± 0.12	64.7

[a] $P < 0.01$ *vs.* control group. [b] $P < 0.05$ *vs.* control group. [c] $P < 0.0001$ *vs.* control group. [d] $P > 0.05$ *vs.* 5-FU group.

Fig. 7, cells without treatment of **B7** (0 nM) exhibited normal arrangement and organizational morphology of the microtubule network. In contrast, cells treated with colchicine (50 nM) exhibited significant disruption of the microtubule network, with aggregation observed around the nucleus. The effects of compound **B7** were found to parallel those of colchicine, as both agents inhibited microtubule polymerization and disrupted microtubule dynamics in a concentration-dependent manner. The results indicate that compound **B7** influences the cellular microtubule network by inhibiting tubulin polymerization, akin to the mechanism of colchicine.

2.3.2 Molecular docking studies. To explore the interaction between **B7** and tubulin, molecular simulation software AutoDock Vina 1.1.2 was utilized for molecular docking to predict the binding mode of **B7** with tubulin (PDB ID: 5YLJ) crystal structure (Fig. 8). The findings revealed that **B7** located at the interface of α/β-tubulin subunits, corresponding to the colchicine-binding site within tubulin, as illustrated in Fig. 8A. The tri-methoxy-benzene ring (ring A) of colchicine nestled in a hydrophobic pocket, composed of residues Ala314, Leu253, and Cys239 (Fig. 8C). And, the ring A of **B7** was deeply embedded into the binding domain, closely overlapping colchicine (Fig. 8B), and establishing extensive hydrophobic interactions with surrounding amino acid residues like Ala314, Leu246, and Lys350. Moreover, binding to the colchicine site of tubulin was maintained by hydrogen-bonding interactions with residues Val236, Val313, and Asn348. Additionally, the *N*-methyl side chain at the C-7 position formed additional hydrogen bonds with residues Asp327 and Gln176, which presumably contribute to the enhanced antitumor activity.

2.4. *In Vivo* research

2.4.1 *In vivo* activity of B7 on tumor growth. Given the impressive *in vitro* antitumor activity and selectivity of compound **B7**, we have decided to proceed with further research on its *in vivo* antitumor activity in a 4T1 Murine breast tumor model. In the 4T1 Murine breast tumor model, BALB/c mice (female) were randomly divided into six groups: negative control group (injected with PBS containing 5% DMSO), **B7**-L group (0.2 mg kg^{-1} **B7**), COL-L group (0.2 mg kg^{-1} colchicine), **B7**–H (0.6 mg kg^{-1} **B7**), COL-H group (0.6 mg kg^{-1} colchicine), and 5-FU (10 mg kg^{-1} 5-Fluorouracil) group, with 6 BALB/c mice

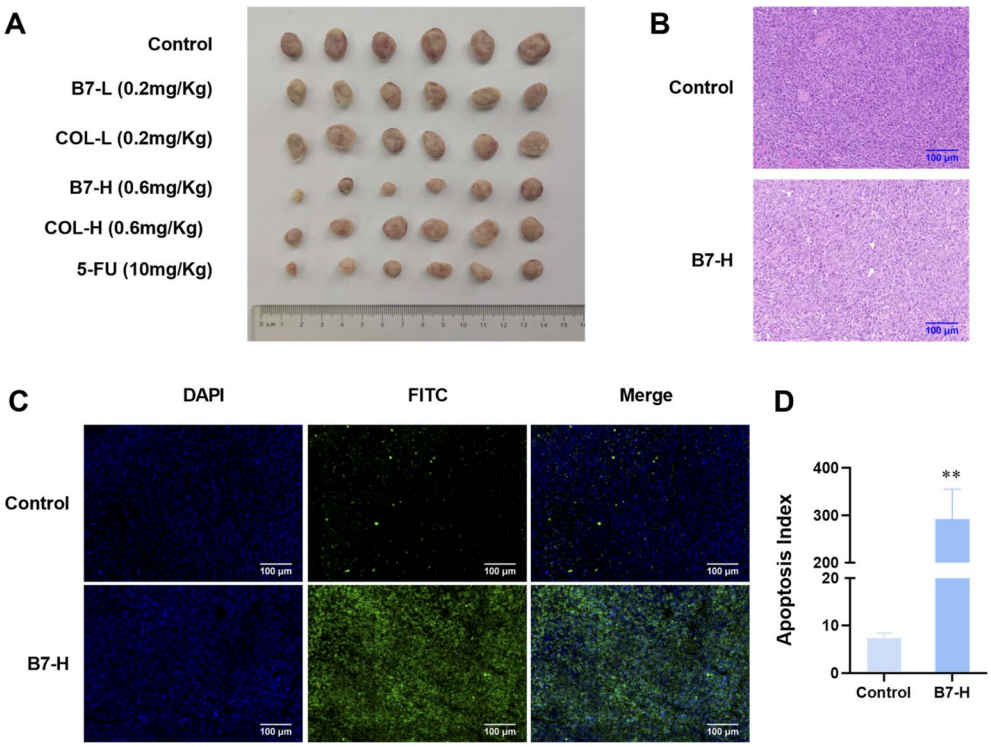

Fig. 9 The effect of compound **B7** on tumor growth in a 4T1 Murine breast tumor model. (A) Morphological images of tumors in each group after administration. (B) Images of tumor sections stained with hematoxylin and eosin (HE). (C and D) Apoptosis and statistical analysis of tumor tissue cells in the **B7**–H group. Compared with the control group, $^{**}P < 0.01$.

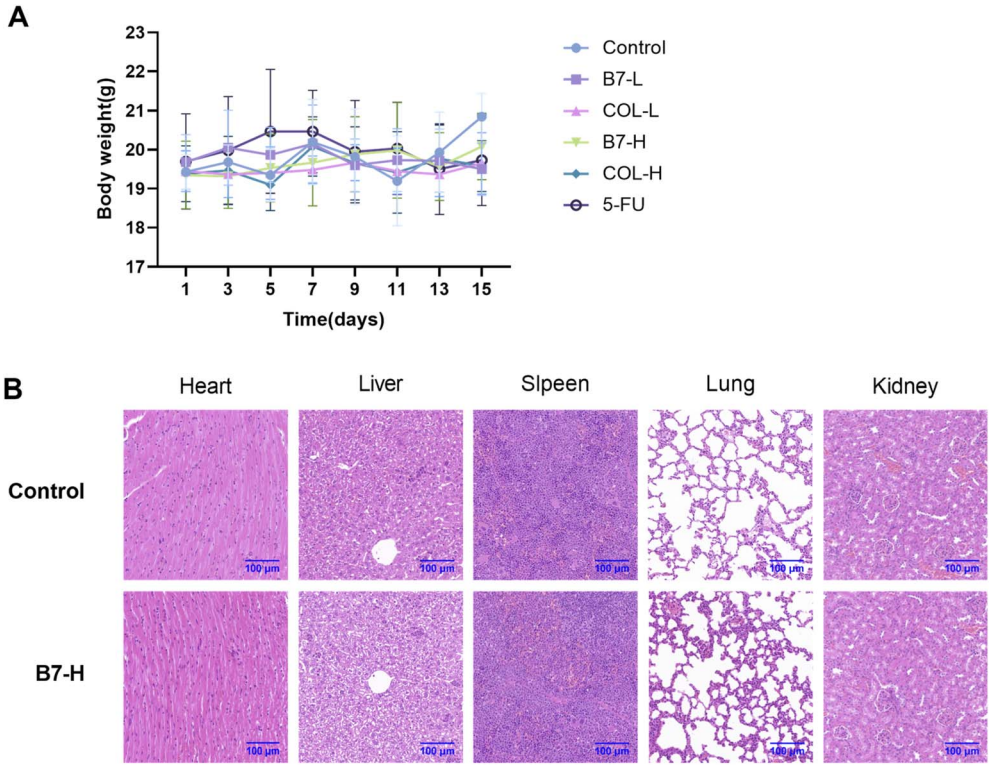

Fig. 10 Safety evaluation of B7 *in vivo*. (A) Changes in body weight of mice in each group during administration. (B) HE staining of the main organs (heart, liver, spleen, lung, and kidney).

in each group. The mice were injected intraperitoneally for 14 consecutive days.

According to Table 3, tumor volumes and weights were significantly reduced in the **B7** treatment groups compared with the negative control group (**B7**-L *vs.* control, $P < 0.01$; **B7**–H *vs.* control, $P < 0.0001$). Furthermore, the tumor growth inhibition rate (TGI) for the **B7**–H group was 68.4%, comparable to the positive control group (5-FU, 64.7%). In contrast, the TGI of the COL-L and COL-H groups was only 20.6% and 33.8%, respectively. These results suggest that compound **B7** has a substantially improved antitumor activity *in vivo* compared to colchicine.

The morphological images of the tumors in each group after administration (Fig. 9A) intuitively demonstrated the remarkable antitumor effect of **B7**. Additionally, HE staining of tumor tissue (Fig. 9B) showed that the group treated with 0.6 mg kg^{-1} **B7** (**B7**–H) had increased intercellular spaces, irregular outlines, and shrunken nuclei. In contrast, the negative control group had closely arranged, plump tumor cells with deep nuclear staining and active mitosis. Moreover, TUNEL staining was performed to detect apoptotic cells, which were labelled green. As illustrated in Fig. 9C and D, the green fluorescence of group **B7**–H was significantly higher than that of the control group, indicating a considerable number of apoptotic cells. The apoptosis index of the control group and the group treated with **B7**–H were 7.28 ± 1.11 and 292.36 ± 62.71, respectively ($P < 0.01$). These results strongly suggest that **B7** treatment can induce apoptosis, leading to tumor cell death.

2.4.2 Safety evaluation of B7. To evaluate the safety of **B7** *in vivo*, body weight was monitored, and the results are shown in Fig. 10A. No significant difference was observed between the control and **B7** administration groups, providing initial evidence of its safety. To further confirm the safety of **B7**, HE staining was performed on key organs, and the results are shown in Fig. 10B. Compared with the control group, no apparent damage was observed in the heart, liver, spleen, lung, or kidney samples from the high-dose group (**B7**–H). These findings conclusively indicate that **B7** has an acceptable safety profile, providing significant reassurance for its subsequent drug development and application.

3 Conclusions

In this study, a series of novel colchicine–cinnamic acid amides (**B1–B12**) with diverse substitutions on the benzene ring of cinnamic acid were designed, synthesized, and fully characterized. These derivatives were subsequently evaluated for their inhibitory activity against multiple cancer cell lines (B16, 4T1, A549, and HepG2) and the normal cell line L929. The results indicated that four derivatives (**B3**, **B6**, **B7**, and **B8**) bearing *para*-position electron-donating substituents displayed markedly enhanced cytotoxicity compared with colchicine. Among them, compound **B7** exhibited the highest selectivity index (SI), substantially exceeding that of unmodified colchicine. Further functional assays demonstrated that **B7** effectively suppressed 4T1 cell proliferation and migration. Mechanistic studies indicated that **B7** disrupts microtubule dynamics, induces G2/M-

phase cell cycle arrest, and triggers apoptosis in 4T1 cells. Molecular docking analysis confirmed the strong binding of **B7** to the colchicine-binding site of tubulin. Importantly, *in vivo* efficacy and safety studies in a solid tumor model support the therapeutic potential of **B7**, highlighting its promise as a lead compound for further development of anticancer agents.

4 Experimental section

4.1. Chemistry

All commercially available reagents were obtained from commercial suppliers and used without further purification. All catalytic experiments were performed under an atmosphere of argon. ^{1}H and ^{13}C NMR spectra were recorded on a 600 MHz NMR spectrometer (JNM-ECZ600R/S1, JEOL, Japan) using TMS as the internal reference, with chemical shifts reported in ppm. Abbreviations used in the NMR follow-up experiments: s, singlet; d, doublet; t, triplet; q, quartet; m, multiple. The LC/Q-TOF mass spectrometer (6546, Agilent, USA) was used for HRMS analysis, yielding mass accuracies consistently below 5 ppm. Analytical runs were performed on a C18 (5 μm, 4.6 mm × 250 mm) column using an LC-20A series HPLC system (Shimadzu, Japan).

4.1.1 Synthesis of *N*-deacetylcolchicine (3). Colchicine (5.00 g, 12.52 mmol), Boc_2O (8.24 g, 37.75 mmol), and DMAP (1.52 g, 12.44 mmol) were dissolved in CH_3CN (30 mL). To this solution, Et_3N (5 mL, 35.97 mmol) was added. The reaction was heated to 90 °C under reflux for 4 h, then additional Boc_2O (8.21 g, 37.62 mmol) was added. After stirring for 20 h, the solution was evaporated to dryness, and ethyl acetate (50 mL) was added; the mixture was then washed with saturated brine (50 mL × 3). The organic layer was dried over Na_2SO_4 and concentrated under a vacuum to yield a brown solid. Purification by column chromatography yielded 3.43 g of *N*-Boc-colchicine.

To a solution of *N*-Boc-colchicine (3.43 g, 6.87 mmol) in CH_3OH (15 mL) was added CH_3ONa (0.75 g, 13.88 mmol) and stirred for 1 h at 0 °C. Then, saturated brine (50 mL) was added, and the target compound was extracted with ethyl acetate (50 mL × 3). The organic layer was combined, dried over Na_2SO_4, and concentrated to crude *N*, *N*′-Boc-deacetylcolchicine.

The crude product was dissolved in 20 mL of a dichloromethane solution of trifluoroacetic acid (50%). After stirring for 3 h at room temperature, the solvent was removed by distillation. To the residue, a sodium bicarbonate-saturated solution was added to adjust the pH to 7–8. The final product, *N*-deacetylcolchicine (**3**), was extracted with CH_2Cl_2 (50 mL × 3), then dried over Na_2SO_4, concentrated under vacuum, and purified by column chromatography (2.14 g, 48% yield). ^{1}H NMR (600 MHz, Chloroform-d) δ 7.70 (s, 1H), 7.16 (d, J = 10.6 Hz, 1H), 6.78 (d, J = 10.7 Hz, 1H), 6.51 (s, 1H), 3.96 (s, 3H), 3.87 (s, 6H), 3.68 (dt, J = 9.9, 5.1 Hz, 1H), 3.62 (s, 3H), 2.45 (dd, J = 13.5, 6.7 Hz, 1H), 2.35 (td, J = 13.0, 6.6 Hz, 1H), 2.28 (t, J = 12.9, 6.3 Hz, 1H), 1.62–1.54 (m, 1H).

4.1.2 General procedure for the colchicine–cinnamic acid amides. To a solution of *N*-deacetylcolchicine (300 mg, 0.84 mmol), cinnamic acid analog (0.84 mmol), and HATU (350 mg, 0.92 mmol) in anhydrous CH_2Cl_2 (4 mL) was added DIPEA (300 μL, 1.68 mmol). After stirring overnight, the reaction mixture was diluted with CH_2Cl_{l2} (25 mL) and washed with 1 N aqueous HCl (30 mL × 3), a sodium bicarbonate-saturated solution (30 mL × 3), and saturated brine (30 mL × 3). The organic layer was dried, concentrated, and purified to yield the colchicine–cinnamic acid amides.

*4.1.2.1. (S)-N-(1,2,3,10-Tetramethoxy-9-oxo-5,6,7,9-tetrahydrobenzo[a]heptalen-7-yl) cinnamamide (**B1**).* Yield 386 mg (94%). HPLC: t_R = 27.696 min, 98.91% purity. ^{1}H NMR (600 MHz, DMSO-d6) δ 8.86 (d, J = 7.5 Hz, 1H), 7.54 (d, J = 7.3 Hz, 2H), 7.45–7.31 (m, 4H), 7.13 (d, J = 3.6 Hz, 1H), 7.11 (s, 1H), 7.02 (d, J = 10.8 Hz, 1H), 6.78 (s, 1H), 6.70 (d, J = 15.8 Hz, 1H), 4.45 (dt, J = 12.0, 7.0 Hz, 1H), 3.85 (s, 3H), 3.82 (s, 3H), 3.78 (s, 3H), 3.54 (s, 3H), 2.61 (dd, J = 13.2, 6.4 Hz, 1H), 2.25 (td, J = 13.2, 7.1 Hz, 1H), 2.08 (t, J = 12.6, 6.4 Hz, 1H), 1.88 (td, J = 12.1, 6.9 Hz, 1H). ^{13}C NMR (151 MHz, DMSO-D6) δ 178.5, 164.8, 164.1, 153.5, 151.3, 151.1, 141.3, 140.2, 135.7, 135.2, 135.0, 134.8, 130.9, 130.2, 129.5, 128.2, 126.0, 121.8, 112.7, 108.3, 61.4, 61.3, 56.6, 56.4, 52.1, 36.2, 29.7. HRMS m/z calc for $C_{29}H_{29}NO_6$ $[M + H]^+$ 488.2068, found 488.2076.

*4.1.2.2. (S, E)-3-(4-Hydroxyphenyl)-N-(1,2,3,10-tetramethoxy-9-oxo-5,6,7,9-tetrahydrobenzo[a]heptalen-7-yl) acrylamide (**B2**).* Yield 201 mg (48%). HPLC: t_R = 21.689 min, 98.15% purity. ^{1}H NMR (600 MHz, Methanol-d4) δ 7.44 (t, J = 5.4 Hz, 2H), 7.42–7.35 (m, 3H), 7.22 (d, J = 11.0 Hz, 1H), 6.78 (d, J = 8.7 Hz, 2H), 6.76 (s, 1H), 6.54 (d, J = 15.7 Hz, 1H), 4.62 (dd, J = 11.9, 6.5 Hz, 1H), 4.00 (s, 3H), 3.90 (d, J = 6.3 Hz, 6H), 3.64 (s, 3H), 2.66 (dd, J = 13.4, 6.3 Hz, 1H), 2.38 (td, J = 13.2, 6.9 Hz, 1H), 2.26 (t, J = 12.9, 6.5 Hz, 1H), 2.03–1.95 (m, 1H). ^{13}C NMR (151 MHz, DMSO-D6) δ 178.5, 165.2, 164.1, 159.6, 153.5, 151.4, 151.0, 141.3, 140.3, 135.7, 135.0, 134.8, 130.9, 129.9, 126.2, 126.0, 118.2, 116.3, 112.7, 108.3, 61.4, 61.2, 56.6, 56.4, 52.0, 36.2, 29.8. HRMS m/z calc for $C_{29}H_{29}NO_7$ $[M + H]^+$ 504.2017, found 504.2025.

*4.1.2.3. (S, E)-N-(1,2,3,10-Tetramethoxy-9-oxo-5,6,7,9-tetrahydrobenzo[a]heptalen-7-yl)-3-(p-tolyl) acrylamide (**B3**).* Yield 310 mg (74%). HPLC: t_R = 30.399 min, 99.64% purity. ^{1}H NMR (600 MHz, Chloroform-d) δ 7.77 (s, 1H), 7.43 (d, J = 10.8 Hz, 1H), 7.39 (d, J = 15.6 Hz, 1H), 7.22 (d, J = 7.7 Hz, 1H), 7.03 (d, J = 7.8 Hz, 1H), 6.94 (d, J = 11.0 Hz, 1H), 6.54 (d, J = 15.9 Hz, 1H), 6.51 (s, 1H), 4.78 (d, J = 9.9 Hz, 1H), 4.01 (s, 3H), 3.95 (s, 3H), 3.89 (s, 3H), 3.69 (s, 3H), 2.55–2.42 (m, 1H), 2.42–2.31 (m, 1H), 2.29 (s, 1H), 2.07–1.96 (m, 1H). ^{13}C NMR (151 MHz, DMSO-D6) δ 178.5, 164.9, 164.1, 153.5, 151.3, 151.1, 141.3, 140.1, 140.0, 135.7, 135.0, 134.8, 132.5, 130.9, 130.1, 128.1, 126.0, 120.8, 112.7, 108.3, 61.4, 61.3, 56.6, 56.4, 52.1, 36.2, 29.8, 21.5. HRMS m/z calc for $C_{30}H_{31}NO_6$ $[M + H]^+$ 502.2224, found 502.2235.

*4.1.2.4. (S, E)-N-(1,2,3,10-Tetramethoxy-9-oxo-5,6,7,9-tetrahydrobenzo[a]heptalen-7-yl)-3-(m-tolyl) acrylamide (**B4**).* Yield 270 mg (64%). HPLC: t_R = 30.434 min, 99.85% purity. ^{1}H NMR (600 MHz, Chloroform-d) δ 7.82 (s, 2H), 7.46 (d, J = 10.8 Hz, 1H), 7.41 (d, J = 15.6 Hz, 1H), 7.15 (q, J = 7.6, 7.0 Hz, 3H), 7.08 (d, J = 8.0 Hz, 1H), 6.96 (d, J = 11.0 Hz, 1H), 6.60 (d, J = 15.6 Hz, 1H), 6.51 (s, 1H), 4.83–4.73 (m, 1H), 4.02 (s, 3H), 3.95 (s, 3H), 3.90 (s, 3H), 3.69 (s, 3H), 2.49 (d, J = 7.3 Hz,1H), 2.36 (t, J = 6.8 Hz, 2H), 2.28 (s, 3H), 2.08–1.98 (m, 1H). ^{13}C NMR (151 MHz, DMSO-D6)

δ 178.5, 164.8, 164.1, 153.5, 151.3, 151.1, 141.3, 140.2, 138.7, 135.7, 135.2, 135.0, 134.8, 130.9, 129.4, 128.7, 126.0, 125.3, 121.7, 112.7, 108.3, 61.4, 61.3, 56.6, 56.4, 52.1, 36.2, 29.7, 21.4. HRMS *m*/*z* calc for $C_{30}H_{31}NO_6$ $[M + H]^+$ 502.2224, found 502.2235.

*4.1.2.5. (S, E)-N-(1,2,3,10-Tetramethoxy-9-oxo-5,6,7,9-tetrahydrobenzo[a]heptalen-7-yl)-3-(o-tolyl) acrylamide (**B5**).* Yield 330 mg (78%). HPLC: t_R = 29.954 min, 99.76% purity. ^{1}H NMR (600 MHz, Chloroform-d) δ 7.90 (d, J = 5.1 Hz, 1H), 7.86 (s, 1H), 7.73 (d, J = 15.5 Hz, 1H), 7.48 (d, J = 10.8 Hz, 1H), 7.44 (d, J = 7.6 Hz, 1H), 7.16 (t, J = 7.3 Hz, 1H), 7.12–7.06 (m, 2H), 6.97 (d, J = 10.9 Hz, 1H), 6.54 (d, J = 15.4 Hz, 1H), 6.52 (s, 1H), 4.80 (dt, 1H), 4.01 (s, 3H), 3.95 (s, 3H), 3.91 (s, 3H), 3.70 (s, 3H), 2.48 (t, J = 10.7 Hz, 1H), 2.41–2.32 (m, 2H), 2.25 (s, 3H), 2.13–2.01 (m, 1H). ^{13}C NMR (151 MHz, DMSO-D6) δ 178.5, 164.8, 164.1, 153.5, 151.3, 151.1, 141.3, 137.6, 137.4, 135.7, 135.1, 134.8, 134.0, 131.2, 130.9, 129.9, 127.0, 126.4, 126.0, 123.0, 112.7, 108.3, 61.4, 61.3, 56.6, 56.4, 52.2, 36.3, 29.7, 19.9. HRMS *m*/*z* calc for $C_{30}H_{31}NO_6$ $[M + H]^+$ 502.2224, found 502.2231.

*4.1.2.6. (S, E)-3-(4-Methoxyphenyl)-N-(1,2,3,10-tetramethoxy-9-oxo-5,6,7,9-tetrahydrobenzo[a]heptalen-7-yl) acrylamide (**B6**).* Yield 326 mg (75%). HPLC: t_R = 27.498 min, 99.66% purity. ^{1}H NMR (600 MHz, Chloroform-d) δ 8.27 (s, 1H), 7.75 (s, 1H), 7.40 (d, J = 10.9 Hz, 1H), 7.32 (d, J = 16.5 Hz, 1H), 7.19 (d, J = 8.1 Hz, 2H), 6.92 (d, J = 11.0, 2.7 Hz, 1H), 6.70 (d, J = 6.1 Hz, 2H), 6.45 (d, J = 16.8 Hz, 2H), 4.86–4.67 (m, 1H), 4.00 (d, J = 2.8 Hz, 3H), 3.93 (d, J = 2.8 Hz, 3H), 3.87 (d, J = 2.8 Hz, 3H), 3.74 (d, J = 2.8 Hz, 3H), 3.69 (d, J = 2.8 Hz, 3H), 2.47–2.41 (m, 1H), 2.39–2.26 (m, 2H), 1.98–1.92 (m, 1H). ^{13}C NMR (151 MHz, DMSO-D6) δ 178.5, 165.1, 164.1, 161.0, 153.5, 151.4, 151.1, 141.3, 139.9, 135.7, 135.0, 134.8, 130.9, 129.8, 127.8, 126.0, 119.3, 114.9, 112.7, 108.3, 61.4, 61.3, 56.6, 56.4, 55.8, 52.1, 36.2, 29.8. HRMS *m*/*z* calc for $C_{30}H_{31}NO_7$ $[M + H]^+$ 518.2173, found 518.2183.

*4.1.2.7. (S, E)-3-(4-(Dimethylamino) phenyl)-N-(1,2,3,10-tetramethoxy-9-oxo-5,6,7,9-tetrahydrobenzo[a]heptalen-7-yl) acrylamide (**B7**).* Yield 350 mg (79%). HPLC: t_R = 29.000 min, 98.16% purity. ^{1}H NMR (600 MHz, Chloroform-d) δ 7.55 (s, 1H), 7.40 (d, J = 15.5 Hz, 1H), 7.32 (dd, J = 9.7, 7.7 Hz, 3H), 6.84 (d, J = 10.8 Hz, 1H), 6.77 (d, 2H), 6.53 (s, 1H), 6.40 (d, J = 15.2 Hz, 1H), 4.77 (dt, J = 12.6, 6.7 Hz, 1H), 3.98 (s, 3H), 3.94 (s, 3H), 3.89 (s, 3H), 3.69 (s, 3H), 3.01 (s, 6H), 2.52 (dd, J = 13.4, 6.4 Hz, 1H), 2.42 (td, J = 13.2, 6.8 Hz, 1H), 2.30 (t, J = 12.8, 6.5 Hz, 1H), 1.90 (td, J = 11.9, 6.9 Hz, 1H). ^{13}C NMR (151 MHz, DMSO-D6) δ 178.5, 165.5, 164.1, 153.5, 151.7, 151.6, 151.1, 141.3, 140.7, 135.8, 135.0, 134.8, 131.0, 129.5, 126.1, 122.6, 116.2, 112.7, 112.5, 108.3, 61.4, 61.3, 56.6, 56.4, 52.0, 40.3, 36.3, 29.8. HRMS *m*/*z* calc for $C_{31}H_{34}N_2O_6$ $[M + H]^+$ 531.2490, found 531.2498.

*4.1.2.8. (S, E)-3-(4-Isopropylphenyl)-N-(1,2,3,10-tetramethoxy-9-oxo-5,6,7,9-tetrahydrobenzo[a]heptalen-7-yl) acrylamide (**B8**).* Yield 336 mg (76%). HPLC: t_R = 36.335 min, 99.41% purity. ^{1}H NMR (600 MHz, Chloroform-d) δ 7.79 (s, 1H), 7.72 (s, 1H), 7.46–7.39 (m, 2H), 7.26 (d, J = 7.6 Hz, 2H), 7.09 (d, J = 7.8 Hz, 2H), 6.94 (d, J = 10.9 Hz, 1H), 6.54 (d, J = 16.2 Hz, 1H), 6.51 (s, 1H), 4.78 (s, 1H), 4.01 (s, 3H), 3.94 (s, 3H), 3.89 (s, 3H), 3.69 (s, 3H), 2.83 (m, J = 6.9 Hz, 1H), 2.50 (d, J = 8.7 Hz, 1H), 2.35 (s, 2H), 2.05–1.96 (m, 1H), 1.20–1.18 (m, 6H). ^{13}C NMR (151 MHz, DMSO-D6) δ 178.5, 164.9, 164.1, 153.5, 151.3, 151.1, 150.8, 141.3, 140.1, 135.7, 135.0, 134.8, 132.9, 130.9, 128.3, 127.5, 126.0, 120.9, 112.7, 108.3, 61.4, 61.3, 56.6, 56.4, 52.1, 36.2, 33.8, 29.8, 24.2. HRMS *m*/*z* calc for $C_{32}H_{35}NO_6$ $[M + H]^+$ 530.2537, found 530.2546.

*4.1.2.9. (S, E)-3-(4-Fluorophenyl)-N-(1,2,3,10-tetramethoxy-9-oxo-5,6,7,9-tetrahydrobenzo[a]heptalen-7-yl) acrylamide (**B9**).* Yield 306 mg (72%). HPLC: t_R = 28.355 min, 99.65% purity. ^{1}H NMR (600 MHz, Chloroform-d) δ 8.35 (d, J = 6.4 Hz, 1H), 7.87 (s, 1H), 7.50 (d, J = 10.8 Hz, 1H), 7.34 (d, J = 15.6 Hz, 1H), 7.26 (q, J = 4.5, 3.6 Hz, 2H), 7.00 (d, J = 10.7 Hz, 1H), 6.90 (t, J = 8.6 Hz, 2H), 6.57 (d, J = 15.6 Hz, 1H), 6.52 (s, 1H), 4.79–4.74 (m, 1H), 4.03 (s, 3H), 3.95 (s, 3H), 3.90 (s, 3H), 3.70 (s, 3H), 2.48 (t, J = 10.1 Hz, 1H), 2.36 (d, J = 6.7 Hz, 2H), 2.06–2.01 (m, 1H). ^{13}C NMR (151 MHz, DMSO-D6) δ 178.5, 164.7, 164.1, 163.3 (J1-CF = 245.4 Hz), 153.5, 151.3, 151.1, 141.3, 139.0, 135.7, 135.0, 134.8, 131.9, 130.9, 130.3 (J3-CF = 21.7 Hz), 126.0, 121.7, 116.5 (J2-CF = 21.7 Hz), 112.7, 108.3, 61.4, 61.3, 56.6, 56.4, 52.2, 38.8, 36.2, 29.7. HRMS *m*/*z* calc for $C_{29}H_{28}FNO_6$ $[M + H]^+$ 506.1973, found 506.1979.

*4.1.2.10. (S, E)-3-(4-Chlorophenyl)-N-(1,2,3,10-tetramethoxy-9-oxo-5,6,7,9-tetrahydrobenzo[a]heptalen-7-yl) acrylamide (**B10**).* Yield 253 mg (58%). HPLC: t_R = 31.563 min, 99.51% purity. ^{1}H NMR (600 MHz, Chloroform-d) δ 8.66 (s, 1H), 7.98 (s, 1H), 7.57 (dd, J = 11.0, 3.2 Hz, 1H), 7.33 (d, J = 15.1 Hz, 1H), 7.22 (d, J = 7.9 Hz, 2H), 7.20–7.14 (m, 2H), 7.07 (d, J = 11.0 Hz, 1H), 6.69 (d, J = 15.9 Hz, 1H), 6.53 (s, 1H), 4.89–4.74 (m, 1H), 4.05 (s, 3H), 3.95 (s, 3H), 3.91 (s, 3H), 3.69 (s, 3H), 2.49 (d, J = 11.3 Hz, 1H), 2.35 (s, 2H), 2.13 (s, 1H). ^{13}C NMR (151 MHz, DMSO-D6) δ 178.5, 164.6, 164.1, 153.5, 151.2, 151.1, 141.3, 138.8, 135.7, 135.1, 134.8, 134.6, 134.2, 130.9, 129.9, 129.5, 126.0, 122.7, 112.7, 108.3, 61.4, 61.3, 56.6, 56.4, 52.2, 36.2, 29.7. HRMS *m*/*z* calc for $C_{29}H_{28}ClNO_6$ $[M + H]^+$ 522.1678, found 522.1685.

*4.1.2.11. (S, E)-3-(3-Nitrophenyl)-N-(1,2,3,10-tetramethoxy-9-oxo-5,6,7,9-tetrahydrobenzo[a]heptalen-7-yl)acrylamide (**B11**).* Yield 259 mg (58%). HPLC: t_R = 28.588 min, 99.45% purity. ^{1}H NMR (600 MHz, Chloroform-d) δ 8.87 (d, J = 6.2 Hz, 1H), 8.06 (m, 1H), 7.96 (t, J = 1.9 Hz, 1H), 7.74 (s, 1H), 7.49 (dt, J = 7.8, 1.4 Hz, 1H), 7.44 (d, J = 10.9 Hz, 1H), 7.39 (t, J = 7.9 Hz, 1H), 7.23 (d, J = 15.6 Hz, 1H), 7.00 (d, J = 11.0 Hz, 1H), 6.61 (d, J = 15.7 Hz, 1H), 6.54 (s, 1H), 4.72 (dt, J = 11.8, 5.9 Hz, 1H), 4.05 (s, 3H), 3.94 (s, 3H), 3.90 (s, 3H), 3.64 (s, 3H), 2.54 (d, J = 7.3 Hz, 1H), 2.45–2.37 (m, 2H), 2.04 (dd, J = 12.2, 6.3 Hz, 1H). ^{13}C NMR (151 MHz, CHLOROFORM-D) δ 179.6, 164.8, 164.3, 153.7, 152.9, 151.3, 148.5, 141.8, 138.2, 137.22, 136.7, 136.2, 134.3, 133.7, 130.6, 129.6, 125.6, 123.8, 123.4, 122.0, 113.5, 107.5, 61.6, 61.5, 56.6, 56.2, 53.1, 36.6, 30.0. HRMS *m*/*z* calc for $C_{29}H_{28}N_2O_8$ $[M + H]^+$ 533.1918, found 533.1926.

*4.1.2.12. (S, E)-N-(1,2,3,10-Tetramethoxy-9-oxo-5,6,7,9-tetrahydrobenzo[a]heptalen-7-yl)-3-(3-(trifluoromethyl)phenyl) acrylamide (**B12**).* Yield 286 mg (61%). HPLC: t_R = 33.890 min, 99.73% purity. ^{1}H NMR (600 MHz, Chloroform-d) δ 8.28 (d, J = 6.6 Hz, 1H), 7.70 (s, 1H), 7.48 (d, J = 7.7 Hz, 1H), 7.43 (s, 1H), 7.42–7.38 (m, 2H), 7.34 (t, J = 7.7 Hz, 1H), 7.29 (dd, J = 15.6, 1.5 Hz, 1H), 6.94 (d, J = 11.0 Hz, 1H), 6.54 (t, J = 7.8 Hz, 2H), 4.75 (dt, J = 11.9, 6.2 Hz, 1H), 4.02 (s, 3H), 3.95 (s, 3H), 3.90 (s, 3H), 3.68 (s, 3H), 2.57–2.49 (m, 1H), 2.47–2.34 (m, 2H), 1.98 (m, 1H). ^{13}C NMR (151 MHz, Chloroform-d) δ 179.7, 165.2, 164.2, 153.7,

153.0, 151.3, 141.8, 139.3, 137.2, 136.0, 135.6, 134.4, 131.07, 130.9, 130.5, 129.1, 125.9, 125.8, 125.6, 124.4, 124.0 (J1-CF3 = 272.7 Hz), 122.1, 113.3, 107.5, 61.7, 61.5, 56.6, 56.2, 53.1, 36.5, 30.0. HRMS *m*/*z* calc for $C_{30}H_{28}F_3NO_6$ $[M + H]^+$ 556.1941, found 556.1949.

4.2. Biology evaluation

4.2.1 Cell lines and cell culture. B16, 4T1, A549, HepG2, and L929 cells utilized in this study were procured from the Cell Bank of the Chinese Academy of Sciences (Shanghai, China). B16 and 4T1 cells were maintained in RPMI-1640 medium containing 10% fetal bovine serum (FBS, Every Green, China) and 1% penicillin-streptomycin solution (Cytiva HyClone, USA). The DMEM medium (Gibco, USA) was used to culture A549, HepG2, and L929 cells. The cells were incubated at 37 °C under a humidified atmosphere with 5% CO_2.

4.2.2 Cell viability assay. Cell viability was measured by MTT Assay to determine the IC_{50} values of the compounds. Cells were seeded in 96-well plates at a final volume of 100 μL per well at the desired concentration (B16: 3×10^4 mL^{-1}; L929 and 4T1: 4×10^4 mL^{-1}; HepG2 and A549: 5×10^4 mL^{-1}) and incubated overnight for adhesion. Then, the control group was incubated in drug-free culture medium, while the experimental group was treated with test compounds at concentrations up to 10 μM for 72 h. After treatment, the old medium was removed and replaced with 100 μL of fresh basic medium containing 0.5 mg mL^{-1} MTT. The plate was incubated at 37 °C for 4 h. Subsequently, 150 μL of DMSO was added to each well to dissolve the formazan crystals. The quantity of formazan, which is directly proportional to the number of viable cells, was measured by monitoring absorbance at 490 nm with a BioTek Plate Reader. IC_{50} values were determined by non-linear regression analysis using GraphPad Prism 9 (GraphPad Software).

4.2.3 Colony formation assay. 1 mL of single-cell (4T1 cell) suspension (1000 cells per ml) was spread on a 6-well plate for 2 h, and the complete medium (1 mL) containing different concentrations of test compounds or PBS was added. The treatment will last 10 days to make colonies visible, with the medium replaced every 2–3 days. After gently washing with PBS, the cells were fixed in methanol for 20 min, then stained with 0.1% crystal violet for 20 min. Finally, the stained cells were observed under a microscope, photographed, and analysed using ImageJ software (National Institutes of Health) to count colonies with more than 50 cells.

4.2.4 Wound healing assay. 4T1 cells were seeded in 6-well plates, each marked with 3 evenly spaced lines on the back, at a density of 3×10^5 cells per well, and grown to confluence. The wound in the cell monolayer was created in the cell monolayer by scratching with a sterile 200 μL pipette tip perpendicular to the reference lines. Each well was washed twice with PBS before adding 2 mL of basic medium containing varying concentrations of test compounds. Wound-healing progress (cell migration) was observed under a microscope, and images of the marked area were taken at 0, 12, and 24 h. The wound-healing area was calculated using ImageJ software.

4.2.5 Immunofluorescence staining. 4T1 cells were seeded in 4-chamber glass-bottom dishes at a density of 1×10^5 cells per chamber. Following overnight incubation, the cells were treated with varying concentrations of B7 (0, 5, 10, or 15 nM) or with colchicine (50 nM). After 24 hours, the samples were fixed in 4% paraformaldehyde for 15 minutes at 4 °C. For permeabilization, the samples were treated with methanol (−20 °C) for 10 minutes at 4 °C. The QuickBlock™ Blocking Buffer (PS108, Epizyme) was used to block for 30 min at room temperature. The primary antibody against Beta Tubulin (GB15140-100, Servicebio) was diluted to a working solution of 1 : 1000 and applied to the samples, followed by overnight incubation at 4 °C. TBST buffer (1×) was used for washing, followed by a FITC-conjugated secondary antibody (SF131, Solarbio) diluted (1 : 200) and applied to the samples. Incubation occurred at room temperature for 1 hour in the dark. To prevent fluorescence quenching and staining of the cell nucleus, a DAPI-sealing agent (BL739A, Biosharp) was applied. Images were then observed and captured using Confocal microscopy (Nikon AX R).

4.2.6 Cell cycle analysis. 4T1 cells were seeded in 6-well plates at 3×10^5 cells per well and incubated overnight. The following day, cells were exposed to various concentrations of **B7** (0, 5, 10, and 15 nM) for 24 h. After digestion with trypsin (without EDTA), the cells were centrifuged at 300 g for 5 minutes and washed with PBS. Then, the cells were fixed overnight with 70% ethanol at −20 °C. This was followed by washing with PBS, and incubation with 100 μL RNase A Reagent (E-CK-A351, Elascience) at 37 °C. Subsequently, the cells were stained with 400 μL of PI reagent (50 μg mL^{-1}, E-CK-A351, Elascience) and incubated in the dark at 4 °C for 30 minutes. At last, the cells were rewashed with PBS, and 200 μL of loading buffer was added for immediate detection by flow cytometry (FongCyte™, challenbio). ModFit LT 5.0 software (Verity Software House) was utilized to analyse the distribution of 4T1 cells at various stages of the cell cycle.

4.2.7 Cell apoptosis assay. 4T1 cells of exuberant growth were plated at a density of 3×10^5 cells per well in 6-well plates. After attachment overnight, different concentrations of **B7** (0, 5, 10, and 15 nM) were treated in the cells for 24 h, then the cells were digested with trypsin (without EDTA), followed by centrifugation at 300 g for 5 minutes. The cells were washed with PBS and resuspended in a Binding Buffer (E-CK-A211, Elabscience). Annexin V-APC and PI reagents (E-CK-A211, Elabscience) were added to detect apoptosis, and the cells were incubated in the dark at room temperature for 10 min. The stained cells were immediately analysed using flow cytometry (FongCyte™, challenbio). The percentage of intact and apoptotic cells was calculated by FlowJ software (TreeStar Inc).

4.3. Molecular docking

The 3D structures of the molecules were drawn using MolView 2.4.6, and the optimized conformation was exported as an SDF file. This file was then converted to PDB format using Open Babel 2.3.2 to retrieve the receptor protein from the PDB repository. The tubulin (PDB ID: 5YLJ) protein structure was

downloaded from the Protein Data Bank (PDB; http://www.rcsb.org/). Using PYMOL 2.3.4, a meticulous cleaning process was performed on the receptor protein, which involved removing water molecules and all bound ligands. To further refine the receptor protein, AutoDockTools was used to add hydrogen atoms and adjust partial atomic charges, yielding an electrically neutral, biologically relevant conformation for molecular docking. The receptor and the ligand were then converted into PDBQT format. The molecular docking was performed with AutoDock Vina 1.1.2, and the resulting complex was visualized using Discover Studio and PYMOL.

4.4. *In vivo* antitumor activity evaluation

4.4.1. 4T1 murine breast tumor model. All animal experimental procedures were approved by the Institutional Animal Care and Use Committee (IACUC) of the Sichuan Industrial Institute of Antibiotics, Chengdu University, and were performed in accordance with the National Institutes of Health (NIH) Guide for the Care and Use of Laboratory Animals. 36 female BALB/c mice, 6 weeks old, weighing 18–20 g, were purchased from Chengdu Dossy Experimental Animal Co., Ltd. The mice were given one week to acclimate to the controlled conditions of an SPF animal facility, where the ambient temperature was maintained at 24 ± 2 °C and the relative humidity at 50 ± 10%. The 4T1 cells were suspended in PBS and prepared for injection. 100 μL per cell suspension (containing roughly 1×10^7 cells) was then injected subcutaneously into the subcutaneous tissue. Subsequent regular observations were made to monitor tumor growth. Once the tumors reached a diameter of 4–5 mm, the mice were re-randomized and distributed evenly among the negative control, low-dose treatment, high-dose treatment, and positive control groups. This strategic reallocation aimed to mitigate volume disparities that might arise from varying tumor growth within each group.

4.4.2 The animal model grouping and treatment principles. The model mice were randomly divided into 6 groups, with 6 animals in each group. Negative control group (Control): intraperitoneal injection of 100 μL saline containing 5% DMSO, once daily, for a total of 14 days. Low-dose **B7** group (**B7**-L): A solution of compound **B7** was administered *via* intraperitoneal injection at a daily dose of 0.2 mg kg^{-1} for 14 consecutive days. Low-dose colchicine group (COL-L): a solution of colchicine was administered *via* intraperitoneal injection at a daily dose of 0.2 mg kg^{-1} for 14 consecutive days. High-dose **B7** group (**B7**–H): a solution of compound **B7** was administered *via* intraperitoneal injection at a daily dose of 0.6 mg kg^{-1} for 14 consecutive days. High-dose colchicine group (COL-H): a solution of colchicine was administered *via* intraperitoneal injection at a daily dose of 0.6 mg kg^{-1} for 14 consecutive days. Positive control group (5-FU): a solution of 5-fluorouracil (5-FU) was administered *via* intraperitoneal injection at a daily dose of 10 mg kg^{-1} for 14 consecutive days.

Throughout the study, the mice's body weights were recorded every other day, and tumor volumes were measured with a precision digital caliper. The tumor volumes were calculated using the formula: Tumor volume = Length × $Width^2/2$. After 14 days of treatment, all groups of mice were sacrificed. Tumor weight was measured, and tumor tissues and main organs were collected for histological analysis (H&E and TUNEL staining). The relative tumor volume (RTV) was calculated as $RTV = V_t/V_0$, where V_t is the volume at the end of treatment and V_0 is the volume at the beginning of treatment. The tumor growth inhibition (TGI) rate was measured using the formula: TGI (%) = [1 − RTV (treatment group)/RTV (control group)] × 100%.

Ethical statement

The IACUC of Sichuan Industrial Institute of Antibiotics at Chengdu University approved the animal trials (Approval Number: SIIA 20231206). The authors declare they have adhered to the ARRIVE guidelines (https://arriveguidelines.org/).

Author contributions

Xiaoqin Li, Yang Chen, and Shumei Wang conceptualized this study. Xiaoqin Li, Shumei Wang, and Yang Chen contributed to the methodology. Xiaoqin Li performed validation. Xiaoqin Li and Shengqi Deng carried out a formal analysis. Xiaoqin Li and Nan Li performed the investigation. Xiaoqin Li, Lin Zheng, and Yang Chen contributed to the design, synthesis, purification, and characterization of the derivatives. Shengqi Deng and Mei Zhang provided resources. Xiaoqin Li and Nan Li performed data curation. Xiaoqin Li contributed to the preparation of the original draft. Xiaoqin Li, Nan Li, Mei Zhang, Shengqi Deng, Lin Zheng, Yang Chen, and Shumei Wang contributed to writing reviews and editing. Xiaoqin Li contributed to the visualization. Yang Chen and Shumei Wang contributed to supervision and project administration. All authors have given approval to the final version of the manuscript.

Conflicts of interest

The authors declare no conflict of interest.

Abbreviations

B16	Mouse melanoma cell line
4T1	Mouse mammary carcinoma cell line
A549	Human lung carcinoma cell line
HepG2	Human hepatoma cell line
L929	Mouse fibroblast cell line
SAR	Structure–activity relationship
DMAP	4-Dimethylaminopyridine
TFA	Trifluoroacetic acid
DCM	Dichloromethane
Boc_2O	Di-*tert*-butyl dicarbonate
HATU	2-(7-Azabenzotriazol-1-yl)-*N*, *N*, *N*′, *N*′-tetramethyluronium hexafluoro-phosphate
DIPEA	*N*, *N*-Diisopropylethylamine
MTT	Methyl thiazolyl tetrazolium

IC_{50}	Half maximal inhibitory concentration, concentration of a drug that is required for 50% growth inhibition *in vitro*
DAPI	2-(4-Amidinophenyl)-6-indolecarbamidine dihydrochloride
HE	Haematoxylin and eosin
TUNEL	Terminal dUTP nick-end labelling
TGI	Tumor growth inhibition rate

Data availability

The data supporting this article have been included as part of the supplementary information (SI). Supplementary information: supplementary Data 1, Data 2 and Data 3, ^{1}H NMR, ^{13}C NMR and HRMS spectral of the derivatives, supplementary Data 4, IC_{50} Data. See DOI: https://doi.org/10.1039/d5ra09278g.

References

1 F. Bray, M. Laversanne, H. Sung, et al., Global cancer statistics 2022: GLOBOCAN estimates of incidence and mortality worldwide for 36 cancers in 185 countries, *CA Cancer J. Clin.*, 2024, **74**, 229–263.
2 P. De, M. Baltas and F. Bedos-Belval, Cinnamic acid derivatives as anticancer agents-a review, *Curr. Top. Med. Chem.*, 2019, **19**, 1694–1711.
3 R. S. Almeer, A. M. Aref, R. A. Hussein, et al., Abdel Moneim, Antitumor potential of berberine and cinnamic acid against solid Ehrlich carcinoma in mice, *Anti Cancer Agents Med. Chem.*, 2019, **19**, 356–364.
4 C. Cheng, G. Li, G. Zheng, et al., Design and synthesis of cinnamic acid triptolide ester derivatives as potent antitumor agents and their biological evaluation, *Bioorg. Med. Chem. Lett.*, 2022, **67**, 128760.
5 H. Shang, L. Li, L. Ma, et al., Design and synthesis of molecular hybrids of sophora alkaloids and cinnamic acids as potential antitumor agents, *Molecules*, 2020, **25**, 1168.
6 C.-C. Xu, T. Deng, M.-L. Fan, et al., Synthesis and in vitro antitumor evaluation of dihydroartemisinin-cinnamic acid ester derivatives, *Eur. J. Med. Chem.*, 2016, **107**, 192–203.
7 V. Ivasiv, C. Albertini, A. E. Gonçalves, et al., Molecular hybridization as a tool for designing multitarget drug candidates for complex diseases, *Curr. Top. Med. Chem.*, 2019, **19**, 1694–1711.
8 B. Sever, C. Türkeş, M. D. Altıntop, et al., Novel metabolic enzyme inhibitors designed through the molecular hybridization of thiazole and pyrazoline scaffolds, *Arch. Pharm.*, 2021, **354**, 2100294.
9 J. M. Andreu, B. Perez-Ramirez, M. J. Gorbunoff, et al., Role of the colchicine ring A and its methoxy groups in the binding to tubulin and microtubule inhibition, *Biochem.*, 1998, **37**, 8356–8368.
10 H. Nishiyama, M. Ono, T. Sugimoto, et al., 4-Chlorocolchicine derivatives bearing a thiourea side chain at the C-7 position as potent anticancer agents, *Med. Chem. Commun.*, 2014, **5**, 452–458.
11 H. Nishiyama, M. Ono, T. Sugimoto, *et al.*, Synthesis and biological evaluation of 4-chlorocolchicine derivatives as potent anticancer agents with broad effective dosage ranges, *Med. Chem. Commun.*, 2012, **3**, 1500–1504.
12 G. Klejborowska, A. Urbaniak, J. Preto, et al., Synthesis, biological evaluation and molecular docking studies of new amides of 4-bromothiocolchicine as anticancer agents, *Bioorg. Med. Chem.*, 2019, **27**, 115144.
13 N. Bensel, D. Lagnoux, V. Niggli, et al., New C (4)-Functionalized Colchicine Derivatives by a Versatile Multicomponent Electrophilic Aromatic Substitution, *Helv. Chim. Acta*, 2004, **87**, 2266–2272.
14 N. Yasobu, M. Kitajima, N. Kogure, et al., Design, synthesis, and antitumor activity of 4-halocolchicines and their prodrugs activated by cathepsin B, *ACS Med. Chem. Lett.*, 2011, **2**, 348–352.
15 M. Cifuentes, B. Schilling, R. Ravindra, et al., Synthesis and biological evaluation of B-ring modified colchicine and isocolchicine analogs, *Bioorg. Med. Chem. Lett.*, 2006, **16**, 2761–2764.
16 B. Bhattacharyya, D. Panda, S. Gupta, et al., Anti-mitotic activity of colchicine and the structural basis for its interaction with tubulin, *Med. Res. Rev.*, 2008, **28**, 155–183.
17 L. Lebeau, P. Ducray and C. Mioskowski, Simple and efficient conversion of colchicine into deacetylcolchicine, *Synth. Commun.*, 1997, **27**, 293–296.
18 J. D. Bagnato, A. L. Eilers, R. A. Horton, et al., Synthesis and characterization of a cobalamin− colchicine conjugate as a novel tumor-targeted cytotoxin, *J. Org. Chem.*, 2004, **69**, 8987–8996.